Let $\mathcal{G}$ be the group and $C(\mathcal{G})$ its Casimer operator. Consider a proper subgroup $\mathcal{G}'$ of the group $\mathcal{G}$. It too will have a Casimir operator which is denoted here by $C(\mathcal{G}')$. Now, $C(\mathcal{G})$ and $C(\mathcal{G}')$ commute and thus will have a common set of eigenfunctions. Then, either the eigenvalues of $C(\mathcal{G}')$ suffice to assign a unique label to each one of the N degenerate states of $C(\mathcal{G})$ or some of the states are still degenerate. In the former case we identify $AC(\mathcal{G}')$ as the algebraic Hamiltonian for the physical problem. In the latter case there will be a proper subgroup $\mathcal{G}''$ of $\mathcal{G}'$ (itself a proper subgroup of $\mathcal{G}$). We then write the algebraic Hamiltonian as a linear combination of $C(\mathcal{G}')$ and $C(\mathcal{G}'')$. If necessary, the procedure is continued until one has a complete set of commuting Casimir operators.

To reiterate, the super Hamiltonian is the Casimir operator of the full group. It therefore commutes with all the generators (and all functions thereof). Starting with an eigenfunction of the super Hamiltonian, the action of the generators will yield the other (degenerate) eigenfunctions. The eigenvalue of the Casimir operator of the group is not the energy but identifies the physical system. As an example, in the Morse oscillator problem (section 8), $N(N-1)$ is the eigenvalue of the Casimir operator of $U(2)$ while m, $m = N - 2v$, is the eigenvalue of the Casimir operator of the proper subgroup $U(1)$, $U(2) \supset U(1)$. The physical energy is Am^2. States are thus labeled by N and m (or N and v).

When the physical Hamiltonian is a linear combination of Casimir operators of a chain of subgroups

$$\mathcal{G} \supset \mathcal{G}' \supset \mathcal{G}'' \ldots \tag{10.3}$$

then the eigenvalues of the Casimir operators of the subgroups serve as good quantum numbers. One can conceive however of a more general case where the Hamiltonian is a general linear combination of linear and bilinear (and even higher order terms) in the generators of the group $\mathcal{G}'$. By construction, such a Hamiltonian will still commute with the Casimir operator of the group $\mathcal{G}$ (i.e. with the super Hamiltonian $\mathcal{H}$ will continue to have common eigenfunctions. Under such circumstances however the subgroups will no longer be symmetry groups of H. In this fashion one can build up algebraic Hamiltonians with any "amount" of desired symmetry. A very practical way of doing this is as follows. Let both $\mathcal{G}'$ and $\mathcal{G}''$ be distinct proper subgroups of $\mathcal{G}$ and let $\mathcal{G}'''$ be a proper subgroup of both $\mathcal{G}'$ and $\mathcal{G}''$

$$\mathcal{G} \supset \left\{ \begin{matrix} \mathcal{G}' \\ \mathcal{G}'' \end{matrix} \right\} \supset \mathcal{G}''' \tag{10.4}$$

Then the Hamiltonian

$$H = A'C(\mathcal{G}') + A''C(\mathcal{G}'') + A'''C(\mathcal{G}''') \tag{10.5}$$

necessarily commutes with the Casimir operator, $C(\mathcal{G}''')$, since $\mathcal{G}'''$ is a proper subgroup of both $\mathcal{G}'$ and $\mathcal{G}''$. Hence, the eigenvalues of $C(\mathcal{G}''')$ remain good quantum numbers. Another scheme is when $\mathcal{G}'$ has two distinct proper subgroups

$$\mathcal{G} \supset \mathcal{G}' \supset \left\{ \begin{matrix} \mathcal{G}'' \\ \mathcal{G}''' \end{matrix} \right. \tag{10.6}$$

Then for a Hamiltonian of the form (10.5) only the eigenvalues of $C(\mathcal{G}')$ are good quantum numbers. In this fashion it is possible to generate spectra which are neither regular (complete set of good quantum numbers) nor completely irregular (no good quantum numbers) but are of intermediate character (some good quantum numbers). It has generally been our experience[30] that most observed molecular spectra are of the latter type.

Finally, we need to mention that the Rayleigh–Ritz variational principle can be used to determine the spectrum of a Hamiltonian bilinear in the generators. Given some reference state ψ_0, the class of trial wave functions is taken to be $T(\mathbf{g})\psi_0$, where T is an element of the group, and the set, $\mathbf{g}$, of group parameters is to be used as the variational parameters. This yields[33] a self-consistent Hamiltonian h which is the very one introduced on dynamical grounds in section 5.

Acknowledgment. The work reported herein reflects many useful discussions with N. Z. Tishby, S. Alexander, and C. E. Wulfman. I thank the members of the Physics Department of Drexel University for their kind hospitality, while this paper was written, and the Stein Foundation for support of my visit there.

(33) N. Z. Tishby and R. D. Levine, *Chem. Phys. Lett.*, **104**, 4 (1984).

Photoelectron Spectra of Transition-Metal–1-Methylborinato Complexes in the Outer Valence Region. Semiempirical Model Calculations Based on Green's Function Formalism[1]

Michael C. Böhm,[†] Rolf Gleiter,*

Institut für Organische Chemie der Universität, D-6900 Heidelberg, West Germany

Gerhard E. Herberich, and Bernd Hessner

Institut für Anorganische Chemie der Technischen Hochschule, D-5100 Aachen, West Germany

(Received: August 8, 1984)

The electronic structures of the 1-methylborinato complexes of $V(CO)_4$ (**1**), $Mn(CO)_3$ (**2**), $Co(CO)_2$ (**3**), and $Co(C_4H_4)$ (**4**) have been studied by means of INDO calculations and their He I photoelectron (PE) spectra. The calculated rotational barriers and the orbital sequences of **1–3** have been compared with their isovalent $(C_5H_5)M(CO)_n$ species. The measured ionization energies are discussed on the basis of those calculated by means of the Green's function formalism. It is found that Koopmans' theorem is only valid in the case of **1**. Significant differences between the filling scheme of the canonical MO's in the ground state and the sequence of the ionic states are demonstrated for **2–4**. It is shown that large relaxation energies are partially compensated by pair-relaxation contributions (i.e., many-body corrections).

I. Introduction

The electronic structures of various transition-metal carbonyl derivatives have been rationalized in the past decade by means of semiquantitative models that were developed on the basis of simple one-electron calculations based on the Wolfsberg–Helmholtz (WH) or extended Hückel (EH) approximation.[3,4] Mo-

[†] Present address: Institut für Physikalische Chemie, Physikalische Chemie III der TH Darmstadt, D-6100 Darmstadt, West Germany.

(1) Part 28 in the series: Electronic Structure of Organometallic Compounds; for part 27 see ref 2.

0022-3654/85/2089-2129$01.50/0

lecular orbital (MO) schemes are available for organometallic fragments with two,[5,6] three,[7-9] and four[10] carbonyl functions. These simplified descriptions have been used to explain the metal–ligand interactions, geometrical preferences, and bonding capabilities in the metal–carbonyl systems.

In the case of organic molecules it is a straightforward procedure to examine the validity of theoretical MO descriptions by means of photoelectron (PE) spectroscopy[11,12] due to an approximate one-to-one correspondence in the outer valence region between the measured ionization potentials (IP's) and canonical molecular orbital energies. It is the well-known Koopmans' theorem[13] ($I_{v,j} = -\epsilon_j$) that relates MO energies derived for the electronic ground state of the N electron system to the vertical ionization energies of the studied compound.

This simple relation between calculated and experimental IP's is not fulfillled in transition-metal compounds where large reorganization effects are often responsible for significant differences between the measured sequence of the ionization potentials and the ordering scheme of the MO's in the electronic ground state.[14-16] In previous contributions we have shown that the importance of these reorganization energies, which can be divided into relaxation corrections in the framework of the Hartree–Fock (HF) approximation and into correlation parameters beyond the independent particle model, depends critically on various molecular parameters (e.g., localization properties of the orbital wave functions, magnitude of the electron–electron interaction integrals, occupation pattern of the transition-metal AO's, energy range of the ionization events, ligand geometries, etc.).[15-20]

Examples for these studies are our investigations of the ground-state and cationic hole-state properties of complexes with the general formula $M(CO)_nL$ (with L indicating an organic ligand and n = 5,[15,21] 4,[22-25] 3,[26-28] 2,[29,30] and 1[31]) by means of theoretical methods that are beyond Koopmans' theorem for the assignment of the PE spectra. The computational background was an improved INDO version[32] which has been developed to simulate high-quality ab initio calculations on organometallic systems.

In this paper we report our investigations concerning the valence electrons of the 1-methylborinato complexes **1–3** by means of

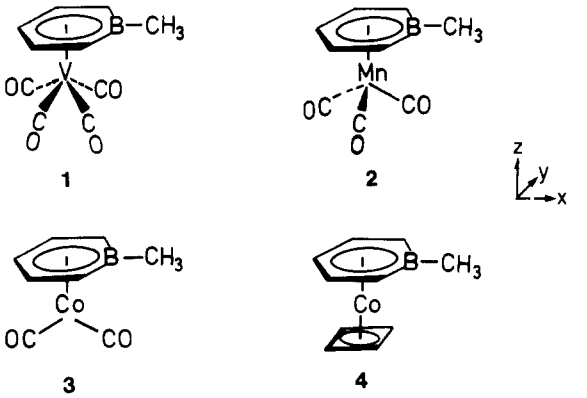

semiempirical calculations using the aforementioned INDO approximation and by carrying out He I photoelectron (PE) measurements. These complexes are ideal models to study (a) the differences and similarities between the 1-methylborinato ligand and the cyclopentadienyl moiety and (b) the modifications of the hole-state properties by changing the central atom from V to Co.

In addition to **1–3** we have recorded the He I PE spectrum of the mixed sandwich **4** to support the assignments derived for **1–3**. The vertical ionization potentials of **1–4** have been calculated by means of the Green's function approach where both relaxation and correlation effects are taken into account. The capability of the method on the ab initio level has been demonstrated in a large number of calculations on small organic molecules.[33,34] The prohibitive computational expense of many-body perturbation theory in combination with large-scale ab initio bases has limited the application of the method in the transition-metal area to small three-atomic species.[35]

The theoretical background of the Green's function formalism is shortly reviewed in the next paragraph. We have employed an approximation for the self-energy part that allows for a fragmentation of the net reorganization energies into relaxation effects on the level of the HF approximation, into the loss of ground-state pair correlation due to the transition from the N electron system to the $(N-1)$ hole state (pair removal), and into the modification of the pair correlation in the $(N-1)$ state as many-body response to electronic relaxation processes (pair relaxation). The ground-state properties of the 1-methylborinato complexes and of **4** are discussed in section III. The He I spectra of **1–4** and the calculated ionization energies are presented in section IV.

II. Theoretical Background

The basic principles of the Green's function approach have been derived in several contributions.[33-37] In analogy to our previous studies we have adopted two approximations for the determination of the self-energy part $\Sigma(\omega)$ in the inverse Dyson equation.[38] $\Sigma(\omega)$ is conveniently defined by the infinite summation displayed in

$$\Sigma(\omega) = \Sigma^{(2)}(\omega) + \Sigma^{(3)}(\omega) + \ldots + \Sigma^{(\infty)}(\omega) \qquad (1)$$

(2) R. Gleiter, M. C. Böhm, and R. D. Ernst, *J. Electron Spectrosc. Relat. Phenom.*, **33**, 269 (1984).
(3) R. Hoffmann, T. A. Albright, and D. L. Thorn, *Pure Appl. Chem.*, **4**, 257 (1977), and references cited therein.
(4) R. Hoffmann, *Science*, **211**, 995 (1981), and references cited therein.
(5) D. M. P. Mingos, *J. Chem. Soc., Dalton Trans.*, 602 (1977).
(6) P. Hofmann, *Angew. Chem.*, **89**, 551 (1977); T. A. Albright, R. Hoffmann, J. C. Thibeault, and D. L. Thorn, *J. Am. Chem. Soc.*, **101**, 3801 (1979).
(7) J. K. Burdett, *J. Chem. Soc., Farday Trans. 2*, **70**, 1599 (1974); J. K. Burdett, *Inorg. Chem.*, **14**, 375 (1975).
(8) A. Rossi and R. Hoffmann, *Inorg. Chem.*, **14**, 365 (1975); M. Elian, M. M. L. Chen, D. M. P. Mingos, and R. Hoffmann, *Inorg. Chem.*, **15**, 1148 (1976).
(9) T. A. Albright, P. Hofmann, and R. Hoffmann, *J. Am. Chem. Soc.*, **99**, 7546 (1977).
(10) M. Elian and R. Hoffmann, *Inorg. Chem.*, **14**, 1058 (1975); P. Kubáček, R. Hoffmann, and Z. Havlas, *Organometallics*, **1**, 180 (1982).
(11) J. H. D. Eland, "Photoelectron Spectroscopy", Butterworths, London, 1974; E. Heilbronner and J. P. Maier in "Electron Spectroscopy, Theory, Techniques and Applications", C. R. Brundle and A. D. Baker, Eds., Academic Press, New York, 1977.
(12) R. Gleiter and J. Spanget-Larsen, *Top. Curr. Chem.*, **86**, 139 (1979); R. Gleiter, *Top. Curr. Chem.*, **86**, 197 (1979).
(13) T. Koopmans, *Physica*, **1**, 104 (1934).
(14) A. Veillard and J. Demuynck in "Modern Theoretical Chemistry", Vol. 4, H. F. Schaefer, Ed., Plenum Press, New York, 1977.
(15) M. C. Böhm and R. Gleiter, *J. Comput. Chem.*, **3**, 140 (1982).
(16) M. C. Böhm, *Theor. Chim. Acta*, **61**, 539 (1982).
(17) M. C. Böhm, *J. Chem. Phys.*, **78**, 7044 (1983).
(18) M. C. Böhm, *Chem. Phys.*, **67**, 255 (1982).
(19) M. C. Böhm, *Int. J. Quantum Chem.*, **22**, 939 (1982).
(20) M. C. Böhm, *Ber. Bunsenges. Phys. Chem.*, **86**, 56 (1982).
(21) M. C. Böhm, R. Gleiter, J. Grobe, and D. Le Van, *J. Organomet. Chem.*, **247**, 203 (1983).
(22) M. C. Böhm, *Inorg. Chem.*, **22**, 53 (1983).
(23) M. C. Böhm, R. Gleiter, and W. Petz, *Inorg. Chim. Acta*, **59**, 255 (1982); M. C. Böhm, *Inorg. Chim. Acta*, **61**, 19 (1982); M. C. Böhm, *Inorg. Chim. Acta*, **68**, 63 (1983).
(24) M. C. Böhm, R. Gleiter, T. A. Albright, and V. Sriyunyongwat, *Mol. Phys.*, **50**, 113 (1983).
(25) M. C. Böhm, J. Daub, R. Gleiter, P. Hofmann, M. F. Lappert, and K. Öfele, *Chem. Ber.*, **133**, 3629 (1980).
(26) M. C. Böhm and R. Gleiter, *J. Comput. Chem.*, **1**, 407 (1980); M. C. Böhm, *J. Mol. Struct. (THEOCHEM)*, **87**, 335 (1982).
(27) M. C. Böhm, *J. Mol. Struct. (THEOCHEM)*, **92**, 73 (1983).
(28) M. C. Böhm and R. Gleiter, *Z. Naturforsch. B*, **35**, 1028 (1980).
(29) M. C. Böhm, *Inorg. Chim. Acta*, **62**, 171 (1982).
(30) M. C. Böhm, R. Gleiter, and H. Berke, *J. Electron Spectrosc. Relat. Phenom.*, **31**, 261 (1983).
(31) M. C. Böhm and R. Gleiter, *Chem. Ber.*, **113**, 3647 (1980).
(32) M. C. Böhm and R. Gleiter, *Theor. Chim. Acta*, **59**, 127, 153 (1981).
(33) L. S. Cederbaum and W. Domcke, *Adv. Chem. Phys.*, **36**, 205 (1977), and references cited therein.
(34) W. v. Niessen, L. S. Cederbaum, W. Domcke, and J. Schirmer, in "Computational Methods in Chemistry", J. Bargon, Ed., Plenum Press, New York, 1980, and references cited therein.
(35) W. v. Niessen and L. S. Cederbaum, *Mol. Phys.*, **43**, 897 (1981).
(36) L. S. Cederbaum, *Theor. Chim. Acta*, **31**, 239 (1973); L. S. Cederbaum, *J. Phys. B.*, **8**, 290 (1975).
(37) F. Ecker and G. Hohlneicher, *Theor. Chim. Acta*, **25**, 289 (1972); P. O. Nerbrant, *Int. J. Quantum Chem.*, **9**, 901 (1975).
(38) F. J. Dyson, *Phys. Rev.*, **75**, 486 (1949).

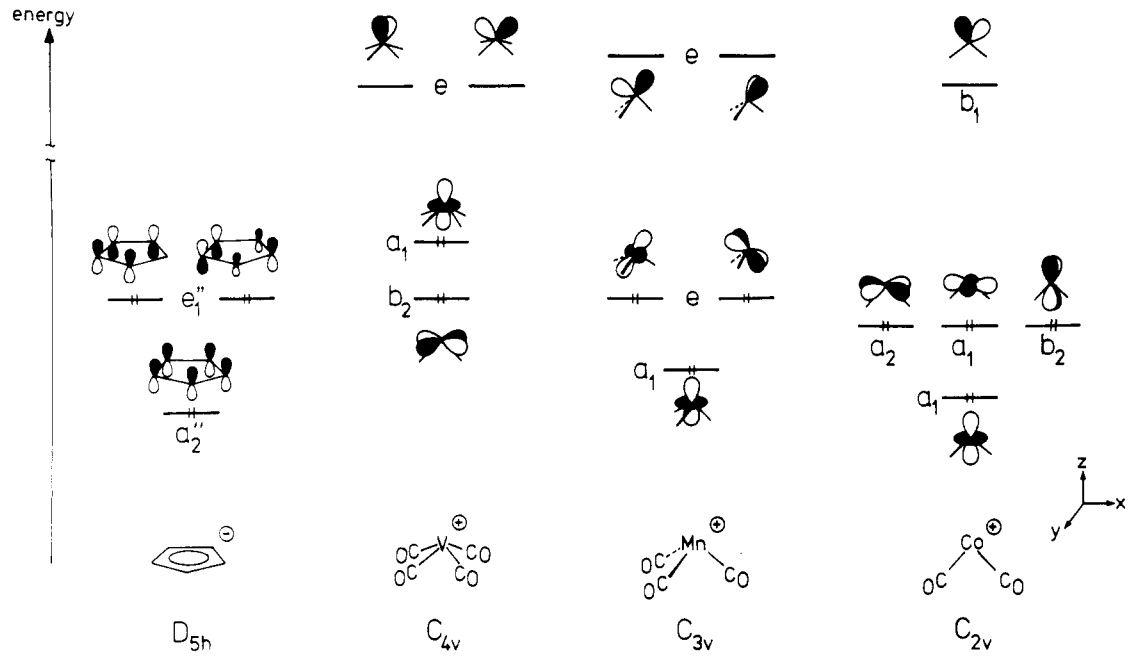

Figure 1. Schematic representation of the highest occupied and lowest unoccupied MO's of $C_5H_5^-$ (D_{5h}), $V(CO)_4^+$ (C_{4v}), $Mn(CO)_3^+$ (C_{3v}), and $Co(CO)_2^+$ (C_{2v}) fragments.

The simplest model potential is given by means of a second-order ansatz for $\Sigma(\omega)$.

$$\text{GF1:} \qquad \Sigma(\omega) = \Sigma^{(2)}(\omega) \tag{2}$$

In the framework of a geometrical approximation for the self-energy operator it is possible to go beyond $\Sigma^{(2)}(\omega)$. Equation 3

$$\text{GF2:} \qquad \Sigma(\omega) = \Sigma^{(2)}(\omega) + \text{D4} \tag{3}$$

corresponds to a renormalized, effective self-energy model and has been derived by Cederbaum for ionization events in the outer valence region.[36] $\Sigma^{\text{eff}}(\omega)$ is given by its second-order contribution, $\Sigma^{(2)}(\omega)$, and a single third-order term, D4 (nomenclature corresponds to that of ref 36), that renormalizes the Koopmans' defects determined by eq 2. The jth vertical ionization energy is related to the jth canonical MO energy and to the different $\Sigma(\omega)$ corrections due to eq 4 and 5 if the inverse Dyson equation is solved

$$-I_{v,j}^{\text{GF1}} = \epsilon_j + \Sigma_{jj}^{(2)}(\omega_j) \tag{4}$$

$$-I_{v,j}^{\text{GF2}} = \epsilon_j + \Sigma_{jj}^{(2)}(\omega_j) + (\text{D4})_{jj} \tag{5}$$

via a diagonal variant. The diagonal self-energy elements summarized in the two equations can be separated into transparent relaxation and correlation increments on the basis of Sinanoğlu's treatment of first-order pair correlations[39] as a lowest-order approximation to the Bethe–Goldstone pairs.[40] This strategy is described in detail in ref 41 and 42. Explicit applications in the transition-metal area with the $\Sigma(\omega)$ potentials of eq 2 and 3 are reported in some of our previous studies.[16,17,22]

The relaxation and correlation elements of the $\Sigma(\omega)$ models of eq 2 and 3 are displayed in

$$\Sigma_{jj}^{(2)}(\omega_j) = R_{jj}^{(2)} + C_{\text{REL},jj}^{(2)} + C_{\text{REM},jj}^{(2)} \tag{6}$$

$$(\text{D4})_{jj} = R_{\text{D4},jj}^{(3)} + C_{\text{D4/REL},jj}^{(2)} \tag{7}$$

$R_{jj}^{(2)}$ describes the relaxation of the $(N-1)$ electrons in the cationic hole state within the one-particle approximation of the HF model in second order of perturbation. $C_{\text{REL},jj}^{(2)}$ is the second-order many-body response to these relaxation effects. It is a pair-relaxation term that takes into account the changes of the pair correlations in the $(N-1)$ system. $C_{\text{REM},jj}^{(2)}$ is called pair-removal energy and is a quantitative measure for the pair correlation disappearing upon removal of the jth electron. Recent theoretical studies, however, have shown that three-hole–two-particle (3h2p) excitations in the jth hole state contribute additionally to the $C_{\text{REM},jj}^{(2)}$ summation which is associated to the N electron system if "classical" definitions for the $\Sigma_{jj}^{(2)}(\omega_j)$ elements are employed.[41-43] The third-order elements $(\text{D4})_{jj}$ can be divided into a relaxation term $R_{\text{D4},jj}^{(3)}$ and into the associated many-body counterpart $C_{\text{D4/REL},jj}^{(3)}$ which is once again a correlation energy of the pair-relaxation type (i.e., associated with the $(N-1)$ electron system). The detailed formulas for the five perturbational summations ($R_{jj}^{(2)}$, $C_{\text{REL},jj}^{(2)}$, $C_{\text{REM},jj}^{(2)}$, $R_{\text{D4},jj}^{(3)}$, and $C_{\text{D4/REL},jj}^{(3)}$) are defined in the literature.[16,22,33,36,41,42]

To solve the inverse Dyson equation we have accepted the same simplifications as in our previous Green's function studies (diagonal approximation for the self-energy part, Taylor series expansion around the Koopmans' pole ϵ_j, Rayleigh–Schrödinger approximation for the third-order elements, $\omega_j \rightarrow \epsilon_j$). In complexes **1–4** we have always employed an array of 14 hole states and 10 particle functions in the perturbational summations that contribute to the self-energy operator $\Sigma(\omega)$.

For the INDO calculations on the 1-methylborinato complexes **1–4** we have used available experimental X-ray data **1**,[44] **2**.[45] The geometrical parameters of **3** have been extrapolated on the basis of the bond lengths and bond angles of **1** and **2**[46] while experimental X-ray values of $(C_5H_5)Co(C_4H_4)$ have been accepted to define the geometry of **4**.[47] Standard bond lengths of 1.1 Å have been adopted for the various CH bonds in complexes **1–4**.[48]

III. Ground-State Properties

To elucidate the electronic structures of **1–3** we first discuss briefly the well-known bonding capabilities of the isovalent electronic species **5–7**. The frontier orbitals of these compounds can be constructed from the π-MO's of the C_5H_5 unit and the

(39) O. Sinanoğlu, *J. Chem. Phys.*, **36**, 706 (1962); O. Sinanoğlu, *Adv. Chem. Phys.*, **14**, 237 (1969).
(40) R. K. Nesbet, *Phys. Rev.*, **155**, 51 (1967); R. K. Nesbet, *Adv. Chem. Phys.*, **14**, 1 (1969).
(41) B. T. Pickup and O. Goscinski, *Mol. Phys.*, **26**, 1013 (1973).
(42) G. Born, H. A. Kurtz, and Y. Öhrn, *J. Chem. Phys.*, **68**, 74 (1978).
(43) J. Schirmer, private communication.
(44) G. E. Herberich, W. Boveleth, B. Hessner, W. Koch, E. Raabe, and D. Schmitz, *J. Organomet. Chem.*, **265**, 225 (1984); E. Raabe, dissertation, Techn. Hochschule Aachen, 1984.
(45) G. Huttner and W. Gartzke, *Chem. Ber.*, **107**, 3786 (1974).
(46) A. Haaland, *Acc. Chem. Res.*, **12**, 415 (1979).
(47) P. E. Riley and R. E. Davies, *J. Organomet. Chem.*, **113**, 157 (1976).
(48) "Tables of Interatomic Distances and Configuration in Molecules and Ions", The Chemical Society, London, 1965, Spec. Publ. No. 18.

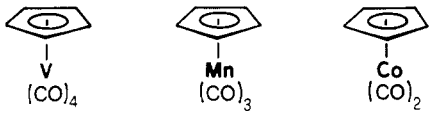

5 6 7

valence MO's of the corresponding $M(CO)_n$ (n = 2–4) units.[10] In Figure 1 we show on the left the π-orbitals of $C_5H_5^-$ and on the right the frontier orbitals of a $V(CO)_4^+$, $Mn(CO)_3^+$, and $Co(CO)_2^+$ fragment. As anticipated there are two, three, and four low-lying occupied valence MO's with large metal admixtures to the one-electron wave functions. The low-lying acceptor orbitals of **5** and **6** are roughly comparable while for $Co(CO)_2$ only one function is found. The lowest unfilled orbitals of $M(CO)_n$ (n = 2–4) (see Figure 1) are ideally suited to stabilize two or one of the highest filled MO's of the C_5H_5 unit.

The shapes of the empty e set in the $V(CO)_4$ and $Mn(CO)_3$ fragment as well as the b_1 orbital of the $Co(CO)_2$ unit have a significant influence on the conformations encountered in the $M(CO)_n$ system. Any significant change in the overlap between these fragment orbitals and the π-levels of the C_5H_5 moiety as a function of the internal rotational angle will cause a barrier. In addition to this HOMO–LUMO interaction we have to take into account the repulsive coupling between filled orbitals of the two fragments. In $V(CO)_4$ no pronounced conformational control is expected, a_1 is of cylindrical symmetry, while a possible influence due to b_2 should be of minor significance as a result of the δ symmetry of this fragment MO. For reasons of symmetry the lower e set of $Mn(CO)_3$ will be important for the conformation of the carbonyl complex. In $Co(CO)_2$ the b_2 combination is prone to interact strongly with the planar π ligand while the two a_1 combinations are once again cylindrically symmetric and a_2 belongs to the δ-type functions.

For all three species a low rotational barrier is predicted since a torsion of the $M(CO)_n$ fragment in **5–7** will not alter the overlap between the HOMO's of the C_5H_5 ligand and the LUMO's of the $M(CO)_n$ unit as a result of the fivefold symmetry of the π-ligand. This is demonstrated below for the $(C_5H_5)Co(CO)_2$ complex in the two conformations A and B. For orientation A

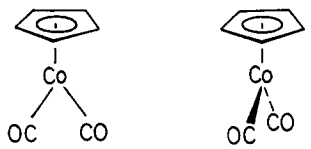

A B

the overlap between the acceptor orbital of the $Co(CO)_2$ unit, b_1, and the corresponding HOMO of the C_5H_5 unit, e_S, is a maximum while for orientation B the e_A linear combination is allowed to overlap with b_1.

The π-MO's of the 1-methylborinato ligand (**8**) can be derived from the π-orbitals of the pentadienyl moiety and the empty 2p function centered at the B–CH_3 unit. The corresponding interaction diagram with the most important coupling schemes is shown in Figure 2. The resulting π-MO's can be looked at as those of a strongly perturbed benzene. A comparison between the MO scheme of the C_5H_5 fragment in Figure 1 and that of **8** in Figure 2 shows the anticipated violation of the cylindrical symmetry of the ligand wave functions and the removal of the degeneracy of the highest filled $e_1''(\pi)$ combination of the C_5H_5 moiety. In analogy to **5–7** the highest occupied MO's of the 1-methylborinato fragment interact preferentially with the acceptor functions of the metal fragment thus stabilizing π_2 and π_3 (see Table I). Just as in the case of **5–7**, the preferred orientation of the methylborinato fragment with respect to the $V(CO)_4$, the $Mn(CO)_3$ and the $Co(CO)_2$ units will be controlled by the interaction between the highest occupied MO's of the ligand orbitals (π_3 and π_2) and the low-lying acceptor orbitals of the metal fragments shown in Figure 1.

The energy split between π_3 and π_2 has a large influence on the different orientations of the $M(CO)_n$ fragment. Due to the closer proximity in energy between π_3 and the empty e or b_1 acceptor orbitals this interaction will determine the conformation. A comparison between π_3 (Figure 2) and the low-lying acceptor MO's (Figure 1) shows a perfect matching of both if one CO group is eclipsed to the B–CH_3 bond in the case of **2** and **3**. For **1** a staggered arrangement between B–CH_3 and the V–CO bonds is preferred. This conformation minimizes the repulsive interaction between the methyl group of the π-ligand and the carbonyl oxygens of the $V(CO)_4$ unit.

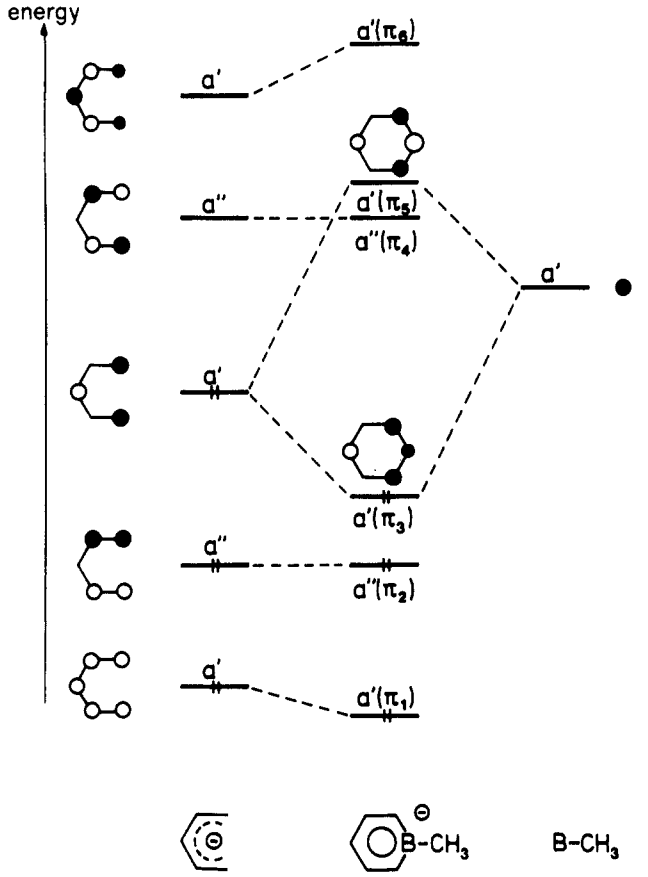

Figure 2. Interaction diagram between the π-MO's of the pentadienyl anion and the empty 2p orbital of a B–CH_3 fragment to yield the π-MO' scheme of the 1-methylborinate ion. The wave functions are labeled with respect to the mirror plane perpendicular to the molecular plane.

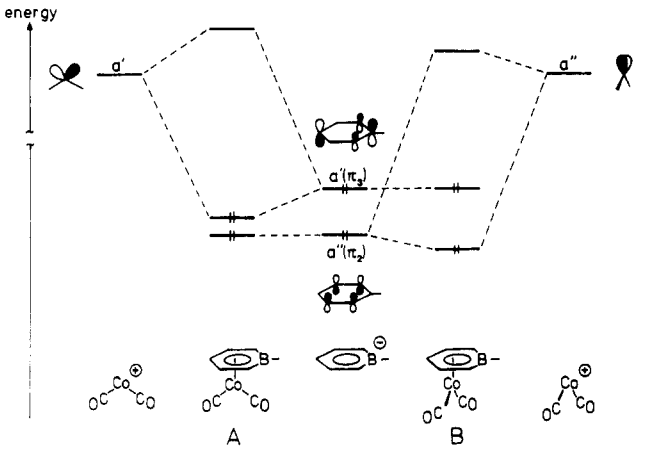

Figure 3. Schematic interaction diagram between the acceptor level of a Co $(CO)_2^+$ unit and the two highest occupied MO's of the 1-methylborinato fragment for the conformations A and B.

In Figure 3 we show as an example the interaction of the methylborinato fragment with the $Co(CO)_2$ moiety in the aforementioned conformations A and B. It is seen that conformation A is preferred over conformation B as a result of the stronger interaction between the acceptor MO and π_3 compared with π_2. This geometrical control via donor–acceptor interactions is reinforced by means of the aforementioned repulsive metal–

TABLE I: Orbital Energies, ϵ_i, MO Type, ($C_5H_5BCH_3$), CO, and Metal Character of the Highest Occupied Molecular Orbitals of the Transition-Metal Polycarbonyl Derivatives $(C_5H_5BCH_3)V(CO)_4$ (1), $(C_5H_5BCH_3)Mn(CO)_3$ (2), and $(C_5H_5BCH_3)Co(CO)_2$ (3) According to INDO MO Calculations[a]

	MO	Γ_i	MO type	ϵ_i, eV	% metal	% L	% CO
1	40	23a′	V $3d_{z^2}$, CO(π)	−9.37	55.8	4.5	39.7
	39	22a′	V $3d_{x^2-y^2}$, CO(π)	−9.61	46.5	10.8	42.7
	38	21a′	L(π), V $3d_{xz}$	−11.06	15.9	75.9	8.2
	37	17a″	L(σ)	−11.17	0.3	98.0	1.7
	36	20a′	L(σ)	−12.32	1.1	97.7	1.2
	35	16a″	L(π), V $3d_{yz}$	−12.60	12.2	78.9	8.9
	34	19a′	L(π), CO(σ)	−13.92	7.6	70.4	22.0
	33	18a′	L(σ), CO(σ)	−14.41	0.4	54.8	44.8
2	36	22a′	L(π), Mn 2e ($3d_{xz}$)	−10.25	15.6	73.8	10.6
	35	14a″	L(σ), Mn 1e ($3d_{xy}$)	−10.31	34.4	58.5	7.1
	34	21a′	Mn 2e ($3d_{x^2-y^2}$)	−10.67	65.8	17.1	17.1
	33	13a″	L(σ), Mn 1e ($3d_{xy}$)	−10.89	32.3	54.5	13.2
	32	20a′	Mn $1a_1$ ($3d_{z^2}$)	−10.94	76.9	10.3	12.8
3	32	11a″	L(π), Co $3d_{yz}$	−9.52	26.9	67.4	5.7
	31	21a′	L(π), Co $3d_{xz}$	−9.59	20.3	75.6	4.1
	30	10a″	L(π)	−10.08	4.0	95.8	0.2
	29	20a′	L(σ), Co $3d_{x^2-y^2}$	−11.23	27.3	70.3	2.4
	28	19a′	Co $3d_{x^2-y^2}$, L(π,σ)	−11.47	54.8	34.5	10.7
	27	18a′	Co $3d_{z^2}$	−11.65	90.0	6.0	4.0
	26	9a″	Co $3d_{xy}$	−11.86	90.2	7.0	2.8
	25	8a″	Co $3d_{yz}$, L(π)	−12.20	54.5	44.6	0.9

[a] The numbering scheme of the irreducible representations (Γ_i) corresponds to the configuration of the valence electrons. L = ($C_5H_5BCH_3$) ligand.

TABLE II: Orbital Energies, ϵ_i, MO Type, ($C_5H_5BCH_3$), (C_4H_4), and Co Character of the Highest Occupied Molecular Orbitals of $(C_5H_5BCH_3)Co(C_4H_4)$ (4) According to the INDO MO Approach[a]

MO	Γ_i	MO type	ϵ_i, eV	% Co	% L	% Cb
32	20a′	L(π), Cb(π)	−9.18	0.8	74.0	25.2
31	12a″	L(π), Cb(π)	−10.08	8.0	54.5	37.5
30	11a″	L(σ)	−10.31	2.7	93.4	3.9
29	19a′	L(σ), Co $3d_{xz}$, Cb (π)	−11.01	27.3	45.8	26.9
28	18a′	Co $3d_{z^2}$, L(π,σ), Cb (π)	−11.43	41.1	34.4	24.5
27	10a″	L(π), Co $3d_{yz}$, Cb (π)	−11.61	34.4	44.1	21.5
26	17a′	L(σ), Co $3d_{z^2}$, Cb (π)	−11.62	38.8	45.5	15.7
25	16a′	Co $3d_{x^2-y^2}$	−12.37	79.5	15.5	15.0
24	9a″	Co $3d_{xy}$	−12.39	93.3	4.2	2.5
23	15a′	L(π), Co $3d_{z^2}$, Cb (π)	−12.61	40.7	41.6	17.7

[a] The numbering scheme of the irreducible representations (Γ_i) corresponds to the configuration of the valence electrons. L, ($C_5H_5BCH_3$) ligand; Cb, (C_4H_4) moiety.

ligand coupling. In addition to the HOMO–LUMO interactions shown in Figure 3 we observe in A a repulsive interaction between the filled b_2 MO of the $Co(CO)_2$ fragment and π_2, while in B, π_3 is destabilized by interacting with the metal fragment. The resulting wave functions are sketched as follows:

π_2-b_2 in A π_3-b_2 in B

By means of hybridization with the empty 4p AO's of Co this interaction can be reduced (i.e., 3d amplitudes are hybridized toward the CO ligands) as follows:

b_2 + 4p

The degree of this deformation depends on the π acidity of the ligand on Co which is stronger in A.

To substantiate these qualitative considerations we have carried out MO calculations using an improved INDO approximation.[32] The following rotational barriers are predicted: **1**, 11.4 kJ/mol; **2**, 28.9 kJ/mol; and **3**; 46.6 kJ/mol. The calculated ground-state conformations of **2** and **3** are consistent with the X-ray structure determinations of $(C_6H_5BC_5H_5)Mn(CO)_3$[45] and of $(C_6H_5BC_5H_5)Co(CO)_2$[44] while for **1** the crystal structure considered by itself would suggest an eclipsed ground-state conformation.[44] As the calculated rotational barrier is very low the observed conformation in the crystal may well be the result of crystal packing effects.

The orbital energies and the types of the orbital wave functions as well as the localization properties of the various MO's of **1–3** are listed in Table I. As can be seen from this table the orbital pattern anticipated qualitatively from the interaction of the two fragments is found, but there are important differences in the sequence of **1–3** and additional features which have to be considered. For **1** we notice that the highest occupied MO's are localized relatively strongly at the metal followed by MO's centered mainly at the π-ligand. For **2** and **3** the highest occupied MO's show a strong methylborinato character while the following MO's are strongly localized at the metal. The HOMO of **3**, e.g., results from the interaction between π_2 and the b_2 fragment orbital of the $Co(CO)_2$ unit which is of $3d_{yz}$ character. As a result of the electropositive B center the calculation predicts high-lying σ-orbitals with a large B participation (see MO's 37 and 38 of **1**). These MO's interact considerably with $3d_{xy}$ (see MO's 35 and 33 of **2** and 29 of **3**) and $3d_{x^2-y^2}$. As an example we show a schematic drawing of 14a″ (MO 35) of **2** and 20a′ (MO 29) of **3**. The one-electron properties of **4** are collected in Table II.

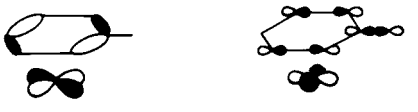

14a″ 20a′

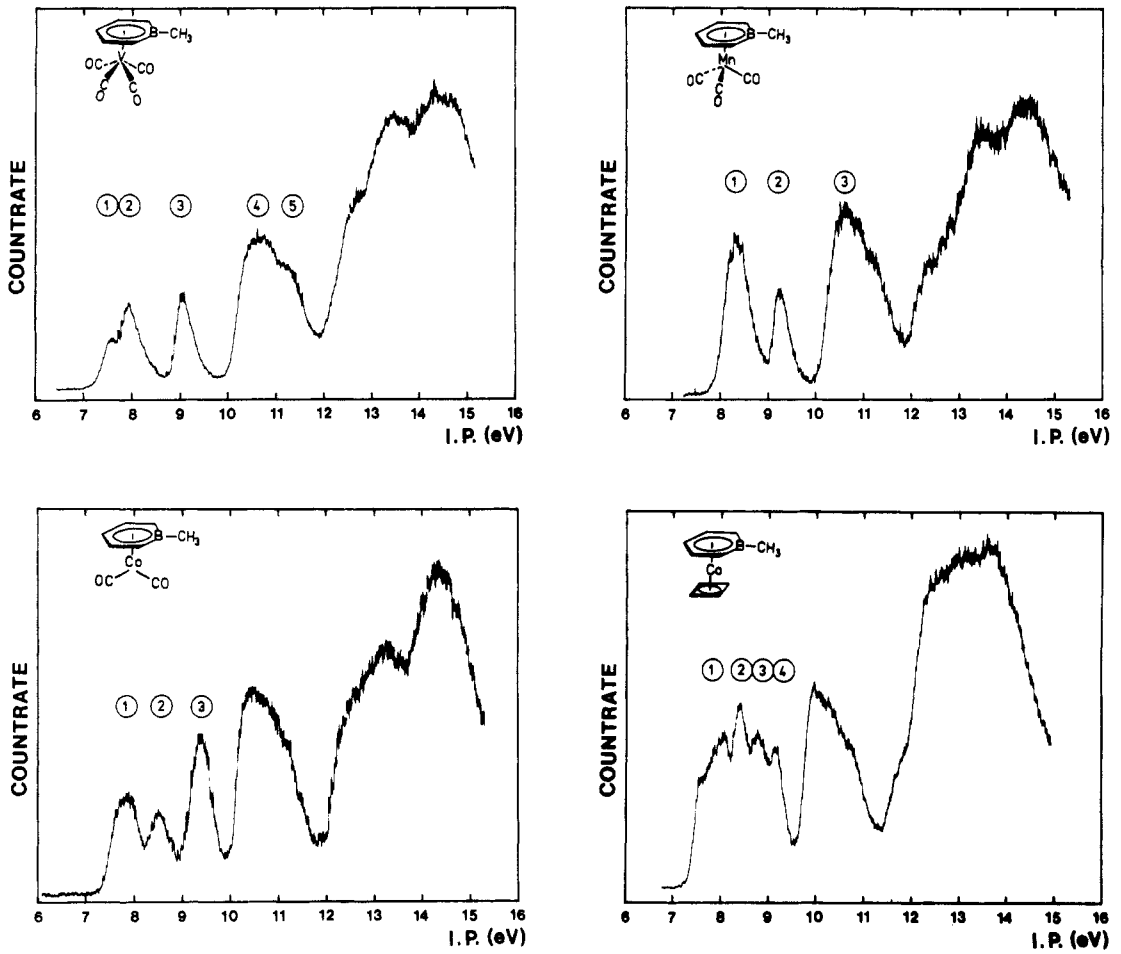

Figure 4. He I photoelectron spectra of **1–4**.

The three highest occupied MO's (20a′, 12a″, and 11a″) are predominantly localized in the six-membered ring. The HOMO (20a′) can be described as an antibonding linear combination between π_3 of **8** (see Figure 2) and the symmetric member of the $1e_g$ HOMO of the C_4H_4 ring. The out-of-phase linear combination between the antisymmetric component of the $1e_g$ HOMO of the C_4H_4 unit and π_2 of **8** is formed by 12a″. The two highest occupied orbitals are followed by 11a″ which is a σ-ribbon orbital of **8**. The next four MO's (19a′, 18a′, 10a″, 17a′) are predicted to be strong mixtures between the high-lying MO's of both ligands and Co 3d functions. The following two MO's (16a′ and 9a′) are strongly localized on the metal.

These results demonstrate that strong metal–ligand interaction and low molecular symmetries lead to strong interaction between all partners. The perturbations of the fragment orbitals are strongest for the cyclobutadiene ligand. From Table II it is seen that the (C_4H_4) admixtures to the MO's of the complex are in any case smaller than 40%. Slightly reduced perturbations are diagnosed for the B ligand; three linear combinations are derived where the ($C_5H_5BCH_3$) admixtures exceed 50%. On the other hand, five complex MO's are predicted in the outer valence region where the heteroligand contributions are found between 35% and 46%. It should be clear that such an interaction pattern leads to a pronounced reduction of the Co 3d amplitudes in those complex MO's that are conveniently called "metal orbitals". Thus only two strongly localized (>80%) MO's are predicted in the mixed sandwich **4**. This splitting pattern differs dramatically from the localization properties of the MO wave functions that are derived in highly symmetrical sandwich compounds (e.g., ferrocene)[53-56] where orbital wave functions are predicted that are either strongly localized at the 3d center or that are typical ligand orbitals with negligible metal admixtures. On the other hand, the INDO results derived for **4** are closely related to the MO properties of boron containing metallocenes[49-51] or sandwich compounds with low molecular symmetries[57] where enlarged metal–ligand interactions are possible due to the larger flexibility of the transition-metal orbitals.

IV. Low-Energy PE Spectra and Hole-State Properties

The He I PE spectra of the three polycarbonyl derivatives **1–3** and of the mixed sandwich **4** are shown in Figure 4. The measured vertical ionization energies of **1–3** are summarized in Table III together with the calculated IP's derived under the assumption of the validity of Koopmans' theorem ($I^K_{v,j}$) and determined in the Green's function formalism with the $\Sigma(\omega)$ approximations defined in eq 2 and 3 ($I^K_{v,j} + \Sigma^{(2)}$, $I^K_{v,j} + \Sigma^{eff}$).

Five peak maxima are found in the outer valence region of the $V(CO)_4$ complex **1** in front of a series of strongly overlapping bands starting at ca. 12.5 eV. Bands 1 and 2 at 7.6 and 7.9 eV belong to a common band system that is separated by 1.1 eV from the third maximum at 9.0 eV. The two remaining maxima at 10.6 and 11.2 eV belong once again to a group of overlapping ionization energies.

(49) D. W. Clack and K. D. Warren, *Inorg. Chem.*, **18**, 513 (1979); *J. Organomet. Chem.*, **208**, 183 (1982).
(50) N. M. Kostić and R. F. Fenske, *Organometallics*, **2**, 1319 (1983).
(51) M. C. Böhm, M. Eckert-Maksić, R. Gleiter, G. E. Herberich, and B. Hessner, *Chem. Ber.*, **115**, 754 (1982).
(52) T. A. Albright and R. Hoffmann, *Chem. Ber.*, **111**, 1578 (1978); T. A. Albright, R. Hoffmann, and P. Hofmann, *Chem. Ber.*, **111**, 1591 (1978).
(53) P. S. Bagus, U. I. Wahlgren, and J. Almlöf, *J. Chem. Phys.*, **64**, 2324 (1976).
(54) M.-M. Rohmer, A. Veillard, and M. H. Wood, *Chem. Phys. Lett.*, **29**, 466 (1974); M.-M. Rohmer and A. Veillard, *Chem. Phys.*, **11**, 349 (1975).
(55) N. Rösch and K. H. Johnson, *Chem. Phys. Lett.*, **24**, 179 (1974); J. Weber, A. Goursot, E. Pěnigault, J. H. Ammeter, and J. Bachmann, *J. Am. Chem. Soc.*, **104**, 4091 (1982).
(56) M. C. Böhm, *Z. Naturforsch. A*, **37**, 1193 (1982).
(57) M. C. Böhm, M. Eckert-Maksić, R. D. Ernst, D. R. Wilson, and R. Gleiter, *J. Am. Chem. Soc.*, **104**, 2699 (1982).

TABLE III: Comparison between the Measured Vertical Ionization Potentials, $I^{expt}_{v,j}$, in the Series 1-3 and Ionization Energies Calculated by Assuming the Validity of Koopmans' Theorem ($I^{K}_{v,j}$) and Using the Green's Function Approach with a Second-Order Approximation to the Self-Energy Part ($I^{K}_{v,j} + \Sigma^{(2)}$) as well as a Renormalized Model Potential ($I^{K}_{v,j} + \Sigma^{eff}$)[a]

compd	band	assignmt	$I^{K}_{v,j}$	$I^{K}_{v,j} + \Sigma^{(2)}$	$I^{K}_{v,j} + \Sigma^{eff}$	$I^{expt}_{v,j}$
1	1	23a′	9.37	8.81	8.89	7.6
	2	22a′	9.61	9.31	9.32	7.9
	3	21a′	11.06	10.61	10.66	9.0
		17a″	11.17	10.62	10.68	
	4	20a′	12.32	11.84	11.89	10.6
		16a″	12.60	12.03	12.09	
	5	19a′	13.92	13.22	13.30	11.2
		18a′	14.41	13.69	13.77	
2	1	20a′	10.94	7.74	8.63	
		21a′	10.67	8.29	8.91	8.3
		14a″	10.31	8.73	9.10	
	2	13a″	10.89	9.36	9.72	9.2
		22a′	10.25	9.76	9.88	
3	1	11a″	9.52	8.37	8.57	
		18a′	11.65	7.90	8.66	7.9
		9a″	11.86	8.23	8.93	
	2	21a′	9.59	9.16	9.19	8.5
		10a″	10.08	9.29	9.39	
	3	19a′	11.47	9.32	9.68	
		8a″	12.20	9.60	10.06	9.4
		20a′	11.23	9.84	10.08	

[a] All values in electronvolts.

On the basis of Tables I and III it seems logical to assign band 1 in the PE spectrum of **1** to the ionization from the HOMO (23a′) while band 2 originates from 22a′. The larger cross section of band 2 compared with band 1 is in line with the reduced V 3d admixtures in 22a′ in comparison with the localization properties of the highest occupied MO.[58] The third peak corresponds to ionization events out of the two ($C_5H_5BCH_3$) ligand orbitals 21a′ and 17a″ which are nearly degenerate. The significant B contributions to the orbital wave functions lead to a reduction of the intensities for the ligand ionization processes.[51] Peaks 4 and 5 are traced back to the MO's 20a′ and 16a″ as well as 19a′ and 18a′. The splitting pattern of the ionization sequence in **1** is well reproduced by the semiempirical INDO approach. The absolute values of the calculated IP's, however, are predicted at too high energies (ca. 1.5 eV). The calculated energy gap of 0.43 eV between the first two IP's must be compared with the measured separation of 0.32 eV. The theoretically predicted separation between the centers of gravity of band 1/band 2 and band 3 (ΔI^{calcd} = 1.57 eV) differs by only 0.3 eV from the measured value of 1.25 eV. The computational results in Table I indicate that the relative separations of the remaining ionization potentials are reproduced with high accuracy.

The INDO results for **1** (Table III) show furthermore that Koopmans' theorem is a sufficient approximation for the assignment of the PE spectrum in the outer valence region. The calculated reorganization energies for ionization processes out of the V 3d MO's 23a′ and 22a′ are smaller than 0.5 eV and are thus comparable with the Koopmans' defects $\Delta I^{K}_{v,j}$ for typical ligand orbitals. Renormalization corrections for the V $3d_{z^2}$ and $3d_{x^2-y^2}$ MO's are negligibly small. The quantum chemical origin for these results has been rationalized in previous studies.[15,17,29]

Two separated peak maxima below 10 eV are found in the PE spectrum of the $Mn(CO)_3$ derivative **2**. The first band at ca. 8.3 eV is comparable with the lowest IP's derived for the isovalent $(C_5H_5)Mn(CO)_3$ complex,[59] and the second maximum at 9.2 eV is closely related to the third band in the PE spectrum of **1**. On the basis of the theoretically determined ionization sequence in the (C_5H_5) derivative of $Mn(CO)_3$[27,59] and due to the comparison with **1** it seems reasonable that peak 1 in the PE spectrum of **2** can be traced back to $1a_1$ and 1e descendants of the $Mn(CO)_3$ valence orbitals (20a′, 21a′, and 14a″) while the second band has to be assigned to the ($C_5H_5BCH_3$) ligand orbitals 13a″ and 22a′.

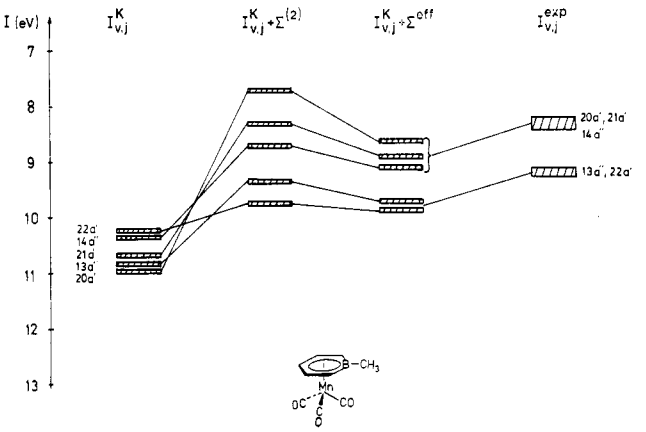

Figure 5. Comparison between the measured vertical ionization potentials of **2**, $I^{expt}_{v,j}$, and calculated values. $I^{K}_{v,j}$ has been derived by assuming the validity of Koopmans' theorem. $I^{K}_{v,j} + \Sigma^{(2)}$ represents a second-order approximation of the self-energy part in the Green's function formalism (GF1) while $I^{K}_{v,j} + \Sigma^{eff}$ represents the renormalized model potential (GF2).

This interpretation is supported by the theoretical results of Table III; a graphic display of the calculated ionization potentials is shown in Figure 5. It is immediately recognized that Koopmans' theorem is not valid in the $Mn(CO)_3$ complex; the sequence of the IP's differs from the MO ordering scheme in the electronic ground state. Significant reorganization energies of 2.31 and 1.76 eV are predicted for ionization processes out of the strongly localized 20a′ and 21a′ orbitals; renormalization effects due to third-order contributions in the $\Sigma(\omega)$ expansion are by no means negligible. The strong metal–ligand coupling between $3d_{xy}$ of the 1e set and σ fragment orbitals of the six-membered π-ring (14a″ and 13a″ linear combinations) leads to a class of one-electron wave functions with reorganization energies that are between the Koopmans' defects of metal ionization processes and ligand ejections. $\Delta I^{K}_{v,j}$ of 14a″ amounts to 1.21 eV while 1.17 eV is predicted for 13a″. The deviation from $I^{K}_{v,j}$ is smallest in the pure ($C_5H_5BCH_3$) σ-orbital 22a′ (0.37 eV). The diagram in Figure

(58) J. W. Rabalais, L. O. Werme, T. Bergmark, L. Karlson, M. Hussain, and K. Siegbahn, *J. Chem. Phys.*, **57**, 1185 (1972); S. Evans, M. L. H. Green, B. Jewitt, A. F. Orchard, and C. F. Pygall, *J. Chem. Soc.*, Faraday *Trans. 2*, **68**, 1847 (1972); C. Cauletti, J. C. Green, M. R. Kelly, P. Powell, J. v. Tilborg, J. Robbins, and J. Smart, *J. Electron Spectrosc. Relat. Phenom.*, **19**, 327 (1980); C. D. Batich, *J. Am. Chem. Soc.*, **98**, 7585 (1976); M. C. Böhm, R. Gleiter, and C. D. Batich, *Helv. Chim. Acta*, **63**, 990 (1980).

(59) D. L. Lichtenberger and R. F. Fenske, *J. Am. Chem. Soc.*, **98**, 50 (1976); T. H. Whitesides, D. L. Lichtenberger, and R. A. Budnik, *Inorg. Chem.*, **14**, 68 (1975).

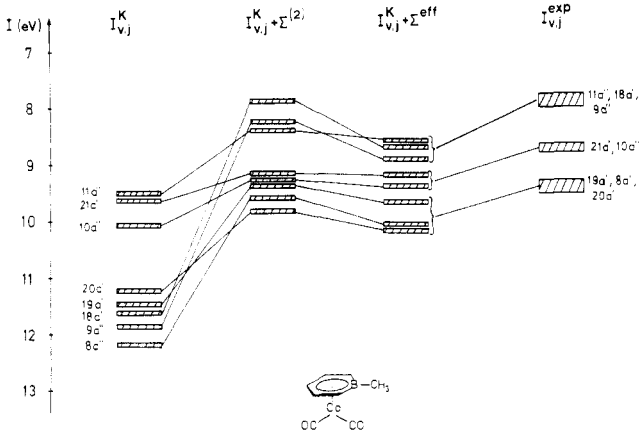

Figure 6. Comparison between measured and calculated ionization energies of **3**; see legend to Figure 5.

5 demonstrates impressively that the gap between the first two maxima is reproduced with high accuracy in the renormalized approximation for the self-energy operator ($\Delta I^{calcd} = 0.92$ eV, $\Delta I^{expt} = 0.9$ eV). The absolute positions of the IP's differ by ca. 0.6 eV.

The PE spectrum of **3** shows three bands below 10 eV (see Figure 4). The comparison with the results of calculations made in Table III suggests assignment of the first and third band to three and the second band to two ionization events. Since two components (18a′, 9a″) assigned to the first band originate from orbitals strongly localized at the Co center the assignment given seems reasonable as a result of the smaller ionization cross sections for metal-centered ionization processes as discussed above. Furthermore the reported PE data of (cyclopentadienyl)(1,4-dimethyl-1,4-dibora-2,5-cyclohexadiene)cobalt[51] and cobaltocene[60] support an assignment where the first maximum is due to ionization events out of strongly localized Co orbitals (18a′ and 9a″).

The Green's function calculations with the renormalized $\Sigma(\omega)$ operator allow for a consistent interpretation of the IP's of **3** (Table III, Figure 6). The ionization energies of 11a″, 18a′, and 9a″ are found in a narrow interval of 0.36 eV between 8.57 and 8.93 eV. The two latter MO's are the aforementioned Co 3d functions that show dramatical deviations from $I^K_{v,j}$ while 11a″ is the HOMO of the $Co(CO)_2$ complex which is less shifted due to the combined effects of relaxation and correlation. The calculated reorganization energies for the Co $3d_{z^2}$ and Co $3d_{xy}$ functions amount to 3.75 and 3.63 eV, respectively, in the second-order approximation of the self-energy part. These defects are reduced to 2.99 and 2.93 eV in the $\Sigma^{eff}(\omega)$ approximation called GF2. The corresponding shifts in the 11a″ HOMO are 1.15 and 0.95 eV. The graphic display in Figure 6 shows that the sequence between 18a′/9a″ and 11a″ is interchanged between the step from GF1 to GF2. It is our opinion that this switch should be traced back to a slight overestimation of the renormalization and that the optimum description lies between GF1 and GF2.

The second band of **3** at 8.5 eV is assigned to electron ejections out of the ($C_5H_5BCH_3$) MO's 21a′ and 10a″. The reorganization energies (0.40 and 0.69 eV) are small in comparison to the $\Delta I^K_{v,j}$ increments of 18a′ and 9a″. Larger relaxation and correlation effects are encountered in the three MO's 19a′, 8a″, and 20a′ that should cause the third maximum in the PE spectrum of **3**. Co admixtures to the orbital wave functions between 27% and 55% are responsible for Koopmans' defects of 2.14 (8a″), 1.79 (19a′), and 1.15 eV (20a′).

The diagram in Figure 6 shows the dramatic difference between the MO sequence in the electronic ground state and the calculated ionization energies derived under the inclusion of relaxation and correlation. The splitting pattern between the three peaks of **3** is reproduced with sufficient accuracy by means of the GF2 approximation (see below); once again a constant shift between

(60) S. Evans, M. L. Green, B. Jewitt, G. H. King, and A. F. Orchard, *J. Chem. Soc., Faraday Trans. 2*, **70**, 356 (1974).

TABLE IV: Comparison between the Measured Vertical Ionization Potentials, $I^{expt}_{v,j}$, of 4 and Ionization Energies Calculated by Assuming the Validity of Koopmans' Theorem ($I^K_{v,j}$) and Using the Green's Function Approach ($I^K_{v,j} + \Sigma^{(2)}$, $I^K_{v,j} + \Sigma^{eff}$)[a] sh = shoulder

band	assignmt	$I^K_{v,j}$	$I^K_{v,j} + \Sigma^{(2)}$	$I^K_{v,j} + \Sigma^{eff}$	$I^{expt}_{v,j}$
1	20a′	9.18	8.97	9.05	7.8sh
	9a″	12.39	7.54	9.07	8.1
	16a′	12.37	8.24	9.47	
2	11a″	10.31	9.52	9.70	
	12a″	10.08	9.73	9.81	8.4
	18a′	11.43	9.20	9.82	
3	17a′	11.62	9.85	10.29	8.8
	19a′	11.01	10.12	10.30	
4	15a′	12.61	9.97	10.73	9.1
	10a″	11.61	10.52	10.75	

[a] See caption to Table III. All values in electronvolts.

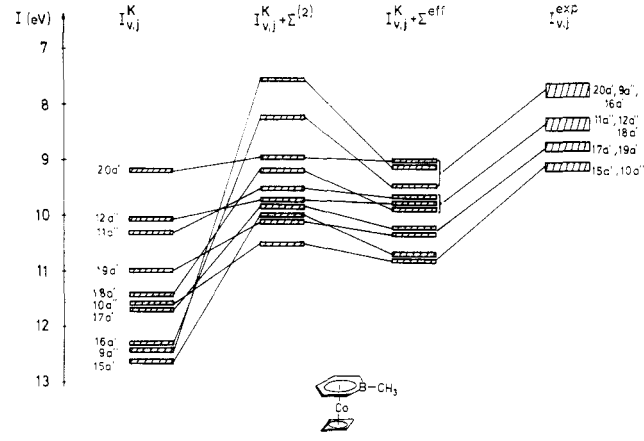

Figure 7. Comparison between measured and calculated ionization energies of **4**; see legend to Figure 5.

measured and calculated IP's has to be taken into account: The ΔI^{calcd} and ΔI^{expt} parameters for band 1/band 2 are 0.57 and 0.6 eV, respectively, while for band 2/band 3 0.65 and 0.9 eV are obtained.

The measured and calculated ionization energies of **4** are collected in Table IV and Figure 7. Four maxima are found in the PE spectrum of **4** below 10 eV. The first band shows a low-energy shoulder at 7.8 eV. To interprete the PE spectrum we rely mainly on the Green's function approach. The results (Table IV) show three closely spaced ionization energies between 9.05 and 9.47 eV which are ascribed to the MO's 20a′, 9a″, and 16a′. Dramatical reorganization energies are predicted for the MO's 9a″ (second order-defect, 4.85 eV; renormalized $I^K_{v,j}$ parameter, 3.32 eV) and 16a′ (4.13 and 2.90 eV, respectively) while negligible corrections are found for the 20a′ HOMO (0.21 and 0.13 eV). In analogy to **3**, we feel that the $\Sigma^{eff}(\omega)$ sequence (20a′ on top of 9a′/16a′) is not correct. The weak low-energy shoulder of peak 1 should be assigned to one of the Co 3d orbitals while the band maximum must be traced back to the HOMO of the mixed sandwich. The measured IP's in this region are thus once again between the second-order approximation GF1 and the renormalized model potential GF2.

Remarkable Koopmans' defects as well as differences in the MO ordering scheme and the IP sequence are also predicted in the remaining bands 2–4. The second peak is assigned to ionization events out of the MO's 11a″, 12a″, and 18a′. Significant Co 3d admixtures are only found in the last one-electron wave function. The calculated Koopmans' defect of 18a′ (1.61 eV) thus exceeds the reorganization energies in the two ligand orbitals (0.61 and 0.27 eV). Peak 3 must be traced back to the MO's 17a′ and 19a′ while the fourth maximum has its origin in 15a′ and 10a″. The theoretically determined $I^K_{v,j}$ parameters are found in an interval between 1.88 eV for the 15a′ combination with 41% Co and 0.71 eV in the 19a′ wave function (27% Co). The various energy gaps between the band maxima are reproduced with high accuracy in the mixed Co sandwich; the absolute differences between calcu-

TABLE V: Decomposition of the Calculated Reorganization Energies (Koopmans' Defects) of 3 and 4 into Relaxation and Correlation (Pair Removal and Pair Relaxation) Elements in the Green's Function Approach[a]

compd	MO	Γ_j	$I^K_{v,j}$	$R^{(2)}_{jj}$	$C^{(2)}_{REL,jj}$	$C^{(2)}_{REM,jj}$	$R^{(2)}_{D4,jj}$	$C^{(3)}_{D4/REL,jj}$	$\Delta I^K_{v,j}$	$I^K_{v,j} + \Sigma^{eff}$
3	27	18a′	11.65	7.11	−3.33	−0.03	−0.73	−0.03	2.99	8.66
	26	9a″	11.86	6.92	−3.22	−0.07	−0.69	−0.01	2.93	8.93
	25	8a″	12.20	3.07	−0.37	−0.09	−0.29	−0.18	2.14	10.06
	28	19a′	11.47	2.67	−0.42	−0.10	−0.25	−0.11	1.79	9.68
	29	20a′	11.23	1.07	0.36	−0.05	−0.10	−0.13	1.15	10.08
	32	11a″	9.52	1.17	0.15	−0.17	−0.10	−0.10	0.95	8.75
	30	10a″	10.08	0.85	0.02	−0.04	−0.05	−0.05	0.69	10.08
	31	21a′	9.59	1.12	−0.26	−0.43	−0.05	−0.02	0.40	9.19
4	24	9a″	12.39	9.44	−4.56	−0.03	−1.50	−0.03	3.32	9.07
	25	16a′	12.37	7.23	−3.00	−0.10	−1.11	−0.12	2.90	9.47
	23	15a′	12.61	2.76	−0.04	−0.08	−0.43	−0.33	1.88	10.73
	28	18a′	11.43	2.36	−0.07	−0.06	−0.37	−0.25	1.61	9.82
	26	17a′	11.62	2.13	−0.15	−0.21	−0.29	−0.15	1.33	10.29
	27	10a″	11.61	1.87	−0.35	−0.44	−0.20	−0.02	0.86	10.75
	29	19a′	11.01	1.17	0.07	−0.35	−0.12	−0.06	0.71	10.30
	30	11a″	10.31	1.18	−0.30	−0.09	−0.14	−0.04	0.61	9.70
	31	12a″	10.08	0.56	0.16	−0.37	−0.06	−0.02	0.27	9.81
	32	20a′	9.18	0.33	0.19	−0.31	−0.05	−0.03	0.13	9.05

[a] The various ionization energies have been assorted with respect to decreasing Koopmans' defects. All values in electrovolts.

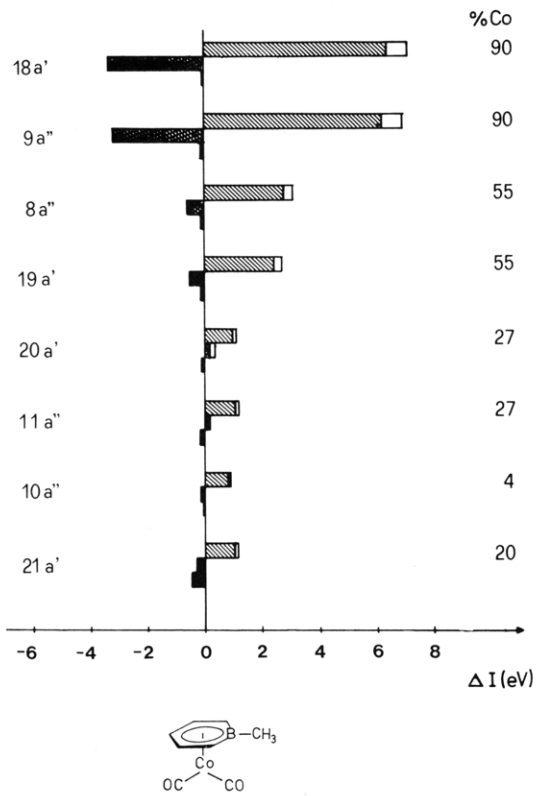

Figure 8. Decomposition of the net reorganization energies in **3** into relaxation and correlation parameters. The first histogram in each triple group corresponds to the relaxation terms $R^{(2)}_{jj}$ and $R^{(3)}_{D4,jj}$. The top of each histogram measures the second-order contributions; the third-order renormalization is symbolized by the blank area. The renormalized relaxation energy is thus defined by the hatched area. The third (black) histogram in the triple groups corresponds to the second-order pair-removal element $C^{(2)}_{REM,jj}$. The pair-relaxation corrections ($C^{(2)}_{REL,jj}$, $C^{(3)}_{D4/REL,jj}$) are displayed in the second member (in the middle). If both elements act in different directions with respect to $I^K_{v,j}$ (i.e., have different signs) we have symbolized the third-order contribution by means of a black area while the effective pair-relaxation energy is given by the hatched area. If both perturbational sums have the same sign the renormalized contribution is defined by the sum of the (hatched) second-order and the (black) third-order corrections. The irreducible representations of the MO's are collected on the left side, the transition-metal admixtures to the MO wave function are shown on the right side.

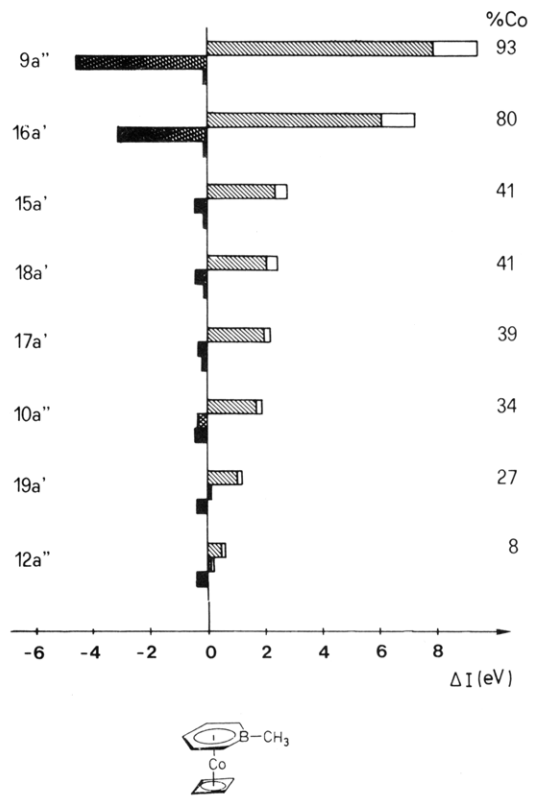

Figure 9. Decomposition of the net Koopmans' defects $\Delta I^K_{v,j}$ of **4** into relaxation and correlation elements. See legend to Figure 8.

lated and measured IP's in **4** are similar to the gaps encountered in the carbonyl derivatives **1–3**. The $I^{calcd}_{v,j}$ and $I^{expt}_{v,j}$ are as follows: band 1/band 2, 0.58 and 0.5 eV; band 2/band 3, 0.52 and 0.4 eV; band 3/band 4, 0.44 and 0.3 eV.

In order to understand the quantum chemical sources leading to the pronounced Koopmans' defects in the Co complexes **3** and **4** we have decomposed the net reorganization energies into the aforementioned relaxation and correlation elements $R^{(2)}_{jj}$, $C^{(2)}_{REL,jj}$, $C^{(2)}_{REM,jj}$, $R^{(3)}_{D4,jj}$, and $C^{(3)}_{D4/REL,jj}$, respectively; the various values are summarized in Table V. Schematic displays of the reorganization contributions are shown in Figures 8 and 9.

It is seen that the second-order relaxation energies are the leading terms in the perturbational expansions for those MO's that are strongly localized at the transition-metal center. The largest $R^{(2)}_{jj}$ values in **3** amount to ca. 7 eV; the ionization energies are of course reduced due to orbital relaxation. The second-order relaxation corrections are still enhanced in the mixed sandwich **4** ($R^{(2)}_{jj,max}$ = 9.44 eV). On the other hand, it is immediately recognized that these strong relaxation phenomena in the cationic hole states are always accompanied by remarkable many-body responses (modification of the pair correlations in the $(N-1)$

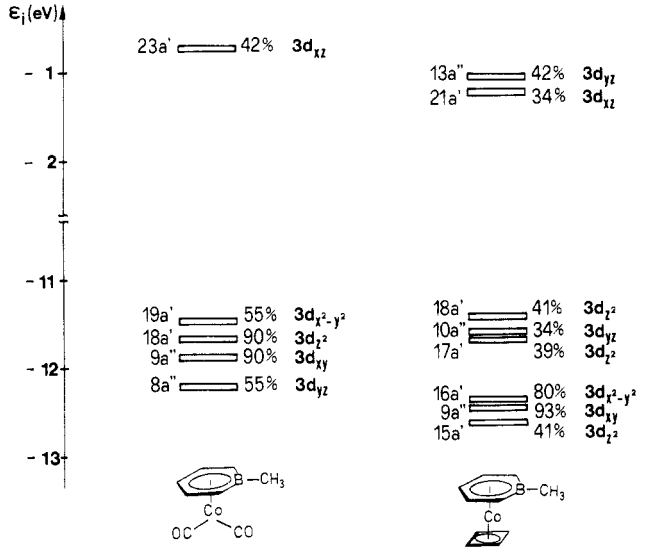

Figure 10. Schematic display of those hole and particle states of **3** and **4** where the transition-metal amplitudes exceed 30%. The two diagrams correspond to semiempirical INDO calculations. The MO's, their localization properties, and the types of the Co 3d AO's are labeled in the figure.

system). $C^{(2)}_{REL,jj}$ acts in an opposite direction to $R^{(2)}_{jj}$ and leads to an increase of the calculated IP's. The ratio between the two elements is −2:1 in the limit of strongly localized orbital (3d) wave functions. The origin of this relation has been analyzed in large detail in previous studies.[16,17] In any case it should be clear that the well-known failures of ΔSCF calculations based on bare ab initio Hamiltonians[61] must be traced back to the neglect of pair relaxation in the cationic hole states.

The influence of $C^{(2)}_{REL,jj}$ is significantly reduced with decreasing localization properties of the orbital wave functions. The Koopmans' defects for MO's with 30–50% Co 3d character are prevailingly determined by orbital relaxation feasible on the stage of the HF approximation. This demonstrates the imbalance between relaxational methods and approaches beyond the independent particle approach as a function of rather small differences in the localization properties of the MO's. Correlation effects (pair relaxation) are more important in the limit of highly localized orbitals.

The loss of ground-state pair correlation is small in comparison to reorganization effects (relaxation and correlation) associated to the $(N-1)$ electron system. The results summarized in Table V and in the Figures 7 and 8, however, indicate that the $C^{(2)}_{REM,jj}$ elements are largest for MO's with 3d amplitudes between 25% and 40%. This $C^{(2)}_{REM,jj}$ magnification has its physical basis in the fact that these correlation energies are determined by a 2p1h (two particle–one hole) summation where always two MO's of the empty Fermi sea are involved in the perturbational expressions. The $C^{(2)}_{REM,jj}$ elements are thus most efficiently accumulated for MO's that are comparable with the low-lying metal acceptor orbitals (i.e., MO's that are strongly mixed metal–ligand functions). A detailed analysis of this behavior is given in ref 19. The important influence of efficient hole–particle excitations that determine the magnitude of the reorganization energies is clearly seen in **3** and **4**. Both comlexes are characterized by occupied Co 3d orbitals with comparable localization properties. The differences in the reorganization elements between the two systems must be traced back to the enhanced hole–particle scattering in **4** where two low-lying acceptor functions with significant 3d amplitudes are predicted (see Figure 10). In the dicarbonyl complex only one Co 3d acceptor is available; the accumulation of relaxation and correlation corrections is thus hindered in the $Co(CO)_2$ derivative in comparison to the mixed Co sandwich.

V. Conclusion

We have demonstrated in this paper that in the series **1–4** the magnitude of orbital reorganization is considerably enlarged in going from **1** to **4**. While in **1** Koopmans' theorem is sufficient to understand the first ionic states, dramatic differences between the MO properties derived for the electronic ground state and calculated ionization potentials have been diagnosed in the Co complexes **3** and **4**. The $Mn(CO)_3$ derivative lies between **1** on one side and **3** and **4** on the other side. We have divided the net reorganization energies into elements of physical significance that allow for a discrimination into relaxation energies and into modifications of pair correlations in the closed-shell ground state and the hole states of the $(N-1)$ systems. This approach allows for a critical theoretical assessment in the transition-metal area where the validity of Koopmans' approximation can be assumed, where purely relaxational methods are a sufficient tool to describe hole-state properties, or where computational techniques beyond the independent particle approach of the HF ansatz have to be employed. Although in **2–4** an approximate one-to-one correspondence between one-electron properties of the ground state and measured ionization energies cannot be assumed it was demonstrated that by knowing the reorganization energies one is able to draw conclusions upon the orbital sequence of the ground state.

VI. Experimental Section

The synthesis of the 1-methylborinato complexes has been described in the literature (**1**,[44] **2**,[62] **3**,[63] and **4**[63]). The He I PE spectra have been recorded on a PS 18 instrument of Perkin-Elmer Ltd. (Beaconsfield, England) and on a UPG 200 spectrometer of Leybold-Heraeus (Köln, Germany). They were calibrated with argon (resolution of the Ar line, 20 meV).

Acknowledgment. This work has been supported by the Stiftung Volkswagenwerk, the Deutsche Forschungsgemeinschaft, the Fonds der Chemischen Industrie, and the BASF Aktiengesellschaft, Ludwigshafen.

Registry No. **1**, 90860-60-9; **2**, 75673-95-9; **3**, 95407-78-6; **4**, 95407-79-7.

(61) M.-M. Rohmer and A. Veillard, *J. Chem. Soc., Chem. Commun.*, 250 (1973); M.-M. Rohmer, J. Demuynck, and A. Veillard, *Theor. Chim. Acta*, **36**, 93 (1974).

(62) G. E. Herberich, B. Hessner, and T. T. Kho, *J. Organomet. Chem.*, **197**, 1 (1980).

(63) G. E. Herberich, H. J. Becker, B. Hessner, and L. Zelenka, *J. Organomet. Chem.*, **280**, 197 (1985).